Exciton Dynamics in CdS−Ag_2S Nanorods with Tunable Composition Probed by Ultrafast Transient Absorption Spectroscopy

Paul Peng,[†] Bryce Sadtler,[†,‡] A. Paul Alivisatos,[†,‡] and Richard J. Saykally*[,†,§]

Department of Chemistry, University of California, Berkeley, California 94720, Materials Sciences Division, Lawrence Berkeley National Laboratory, California 94720, and Chemical Sciences Division, Lawrence Berkeley National Laboratory, California 94720

Received: December 9, 2009; Revised Manuscript Received: February 11, 2010

Electron relaxation dynamics in CdS−Ag_2S nanorods have been measured as a function of the relative fraction of the two semiconductors, which can be tuned via cation exchange between Cd^{2+} and Ag^+. The transient bleach of the first excitonic state of the CdS nanorods is characterized by a biexponential decay corresponding to fast relaxation of the excited electrons into trap states. This signal completely disappears when the nanorods are converted to Ag_2S but is fully recovered after a second exchange to convert them back to CdS, demonstrating annealing of the nonradiative trap centers probed and the robustness of the cation exchange reaction. Partial cation exchange produces heterostructures with embedded regions of Ag_2S within the CdS nanorods. Transient bleaching of the CdS first excitonic state shows that increasing the fraction of Ag_2S produces a greater contribution from the fast component of the biexponential bleach recovery, indicating that new midgap relaxation pathways are created by the Ag_2S material. Transient absorption with a mid-infrared probe further confirms the presence of states that preferentially trap electrons on a time scale of 1 ps, 2 orders of magnitude faster than that of the parent CdS nanorods. These results suggest that the Ag_2S regions within the heterostucture provide an efficient relaxation pathway for excited electrons in the CdS conduction band.

I. Introduction

The size, shape, and chemical composition of semiconductor nanocrystals control their resulting optoelectronic properties. For instance, in both semiconductor alloys and heterostructures, the band gap absorption and emission energies can be widely tuned through the spatial variation of composition.[1−8] The composition of colloidal nanocrystals is typically mediated by the time-dependent variation of cation and anion precursor concentrations during solution-phase nucleation and growth.[1,2] Alternatively, nanocrystals of a desired shape and size can be chemically transformed, postsynthesis, through a solid-state reaction into a new composition. Notably, in ionic nanocrystals, cation exchange can be used to partially or fully replace the cations within the lattice of the crystal with substitutional cations from solution.[6−12] Such solid-state reactions can occur with remarkable efficiency, owing to molecular-like reaction kinetics of nanoscale materials possessing high surface-to-volume ratios.[8−10,13] Furthermore, when the exchange is limited to occur through only a portion of the nanocrystal, heterostructures are produced containing distinct regions of the secondary and host crystals connected by a continuous anion framework.

Several recent reports have characterized the structural and static optical properties of semiconductor nanocrystals produced by cation exchange.[7−11] Transmission electron microscopy (TEM) and X-ray diffraction (XRD) show that the crystals retain their size and shape and are highly crystalline after the exchange reaction. However, such techniques are rather insensitive to local defects that may be introduced, and so far, there has not been a systematic determination of how such chemical transformations affect exciton dynamics in the nanocrystals. There is evidence from related systems that the structural disorder (such as vacancies or substitutional impurities) introduced by the interdiffusion of ions can lead to additional relaxation pathways for photoexcited charge carriers.[14,15]

We report pump−probe measurements in CdS−Ag_2S nanorods to characterize the effect that cation exchange has on the relaxation of excited carriers. We have chosen this material system as the relative fraction of the two semiconductors can be readily controlled by the amount of Ag^+ that is added to the CdS nanorods (or conversely the amount of Cd^{2+} added to Ag_2S nanorods).[8,16] Moreover, the combination of semiconductors that possess a type I (sandwiched) electronic band alignment can lead to the transfer of excited electrons and holes in the wide band gap material (CdS) to the smaller band gap material (Ag_2S), provided that competing relaxation pathways are inhibited.[8] We study carrier relaxation dynamics by monitoring the transient bleaching of the first excitonic transition ($1S_e$), and the intraband absorption ($1S_e-1P_e$) of electrons in the conduction band of CdS nanorods. The change in time constants of the relaxation dynamics following complete and cyclic conversion between CdS and Ag_2S nanorods (i.e., forward conversion from CdS to Ag_2S and back conversion to CdS) is used to characterize how the process of cation exchange can lead to new relaxation pathways through introduction of defect states. Partial cation exchange to make CdS−Ag_2S heterostructures demonstrates how the presence of Ag_2S affects the relaxation of excited carriers in the CdS material.

II. Experimental Methods

A. CdS Synthesis. Colloidal CdS nanorods were synthesized according to previously published procedures.[8,10] A detailed description of the reaction conditions is provided in the

* To whom correspondence should be addressed. E-mail: saykally@berkeley.edu.
[†] University of California, Berkeley.
[‡] Materials Sciences Division, Lawrence Berkeley National Laboratory.
[§] Chemical Sciences Division, Lawrence Berkeley National Laboratory.

10.1021/jp9116722
Published on Web 03/04/2010

Supporting Information. Briefly, cadmium oxide was complexed with propyl- and octadecyl-phosphonic acids in the coordinating solvent, trioctylphosphine oxide, at high temperature under an argon atmosphere to form cadmium-phosphonate. Trioctylphosphine (TOP) and trioctylphosphine sulfide (TOPS) were injected at 320 °C to induce nucleation of the CdS nanorods, which were grown at high temperature for approximately 70 min, during which time additional TOP and TOPS were added slowly via a syringe pump. After cooling the reaction, the nanorods were then washed several times with organic solvents and surfactants to remove the remaining Cd−phosphonate complex. The CdS nanorods were dispersed in toluene and stored in an argon-filled glovebox. While a variety of coordinating molecules are used in the synthesis and subsequent cleaning of the nanorods, previous studies indicate that cadmium chalcogenide nanocrystals grown by such methods are primarily passivated by the alkylphosphonic acids used to control their growth kinetics.[17]

B. Cation Exchange. Ag^+ cation exchange was used to convert CdS nanorods into CdS−Ag_2S nanorod heterostructures and Ag_2S nanorods, using slight modifications to our previous reports.[8] The reactions were performed inside an argon-filled glovebox at room temperature. The extent of conversion can be controlled by the amount of Ag^+ added to a known concentration of CdS nanorods. For Ag^+/Cd^{2+} ratios of 0.50, 1.0, and 1.5, the volume fractions of Ag_2S within the nanorods were 0.12, 0.19, and 0.30 as measured from TEM images. Excess Ag^+ was used for full exchange ($Ag^+/Cd^{2+} > 4$). The molar concentration of Cd^{2+} ions for each CdS nanorod solution was determined by inductively coupled plasma atomic emission spectroscopy of acid-digested samples. Typical molar extinction coefficients used to obtain the Cd^{2+} concentration in the CdS nanorod solutions were 3000 L mol^{-1} cm^{-1} at 300 nm measured by visible absorption spectroscopy. The amount of Cd^{2+} in the CdS nanorod solution for each reaction was between 1×10^{-6} and 3×10^{-6} mol. In a typical reaction, 8 mg of silver nitrate ($AgNO_3$) was dissolved in 3 mL of methanol (MeOH) and was then diluted further with MeOH depending on the desired Ag^+/Cd^{2+} ratio. The $AgNO_3$ solution (∼0.5−1 mL) was added to a larger amount of toluene (∼1−3 mL) so that the nanorods would remain soluble during the reaction. A solution of CdS nanorods in toluene (∼0.15−0.6 mL) was then added to the Ag^+ solution while stirring. The color of the nanocrystal solution changes rapidly (<1 s) from yellow to dark brown after mixing of the Ag^+ and CdS solutions. The converted nanorods were subsequently washed by the addition of MeOH followed by centrifugation and removal of the supernatant. To convert the Ag_2S nanorods back to CdS, a solution of the Ag_2S nanorods was redispersed in tetrahydrofuran and mixed with a large excess of cadmium nitrate ($Cd^{2+}/Ag^+ \sim 100$) dissolved in acetonitrile (MeCN). A drop of tributylphosphine (TBP) was then added and the reaction was heated to approximately 85 °C for 20 min while stirring. The Supporting Information provides further synthetic detail for each of the samples used in these studies.

C. Nanocrystal Characterization. Bright field TEM images were obtained using an FEI Tecnai G2 Supertwin electron microscope operating at 200 kV. TEM samples were prepared by placing a drop of the nanocrystal solution onto a carbon-coated copper grid in ambient atmosphere. Size statistics for the length and diameter of the CdS nanorods before and after cation exchange were determined from TEM images taken at a magnification of 97000× to 195000× using Image-Pro Plus or ImageJ software and making at least 250 measurements. The volume fractions of Ag_2S within the CdS nanorods for different Ag^+/Cd^{2+} ratios were calculated by measuring the size of the Ag_2S regions within 100 nanorods for each sample and estimating their volume from the two-dimensional image. Small Ag_2S regions were approximated as spheres, whereas Ag_2S regions that spanned the diameter of the nanorods were approximated as cylinders.

For absorption and fluorescence measurements, the nanocrystals were precipitated and redispersed in tetrachloroethylene, and placed in a 1 cm path length FUV quartz cuvette with a flat absorption profile from ∼170 to 2200 nm. Absorption spectra were recorded on an Agilent 8453 UV−visible spectrophotometer. Fluorescence spectra were recorded on a Horiba Jobin Yvon Fluorolog 3 equipped with a Triax 320 spectrometer. The excitation wavelength was 400 nm, and a photomultiplier tube was used for detection. The emission spectra were corrected for the wavelength-dependent response of the emission grating and detector and the background of the solvent.

Fluorescence quantum yields were measured by comparing the integrated emission intensity of the nanocrystal sample with that of a reference dye. Coumarin 480 (Exciton Inc.) was used, which has a quantum yield of 74% in ethanol at an excitation wavelength of 390 nm.[18] The optical densities of the solutions were matched at the excitation wavelength and were approximately 0.02 at 390 nm for both the CdS nanorods and the Coumarin 480 dye. The quantum yields were corrected for the refractive index of the solvent and small differences in optical density of the solution.

D. Femtosecond Transient Spectroscopy. A 1 kHz regeneratively amplified titanium:sapphire laser ($\tau = 150$ fs, $\lambda_{center} = 800$ nm) was used for the time-resolved experiments. The majority (90%) of this output pumps a commercial (Light Conversion, TOPAS) optical parametric amplifier or a home-built noncollinear optical parametric amplifier to tune the probe from the visible to the mid-infrared. A normalized transient bleach spectrum obtained with a white light continuum probe determined the lowest excitonic transition for the CdS nanorods to be at an energy corresponding to a probe wavelength of $\lambda =$ 470 nm. Difference frequency generation between the optical parametric amplifier signal and idler photons in a $AgGaS_2$ nonlinear crystal produced the mid-infrared ($\lambda = 4$ μm) probe for intraband absorption experiments, as determined by the energy difference between the $1S_e$ and $1P_e$ levels. The remaining (10%) fundamental output is frequency-doubled ($\lambda = 400$ nm) and used as the optical pump (4 mW, 200 μm spot size) in the experiments. The pump beam path traverses an optical delay line and is also optically chopped at 500 Hz for gated boxcar integrator detection. Either a photodiode or mercury cadmium telluride detector is used to measure the differential probe transmission $\Delta T/T$ as a function of optical delay. A neutral density filter maintained a pump fluence such that, on average, there was less than one electron−hole pair that was excited per nanocrystal, $\langle N_{e-h} \rangle = 0.30 \pm 0.08$, given a 0.8−1.4 range in optical densities and extinction coefficient of 9.3×10^6 cm^{-1} M^{-1}. The nanocrystals were dissolved in toluene and placed in a 1 mm path length NIR cuvette. Between three and five averaged transients represent each of the dynamics traces shown herein, and all experiments were conducted at room temperature.

III. Results and Discussion

A. Transient Bleaching and Absorption Dynamics. As shown in Figure 1, electrons and holes photogenerated above the band gap (so-called hot carriers) in semiconductor nanocrystals typically have the following relaxation scheme: First, intraband relaxation (Figure 1B) of the carriers to the band edge occurs, which can be fast (≤1 ps) depending on the overlap

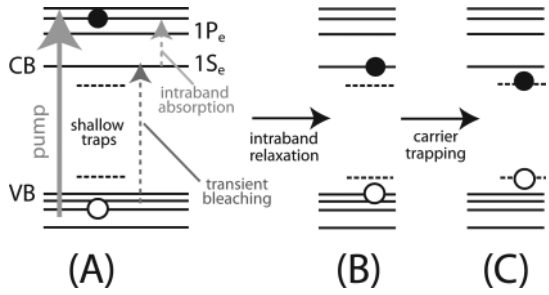

Figure 1. Energy level schemes of parent CdS nanorods and subsequent relaxation pathways: (A) An electron−hole pair is created by the pump pulse ($\lambda_{pump} = 400$ nm); intrinsic shallow and deep trap states are present within the band gap. (B) Rapid intraband relaxation of electron and hole to the band edge follows, and the occupation of the $1S_e$ level can be probed either by transient bleaching ($\lambda_{probe} = 470$ nm) or intraband absorption ($\lambda_{probe} = 4\ \mu$m). If band edge radiative recombination does not occur, then (C) further trapping of the hole into shallow/deep traps can lead to trap relaxation.

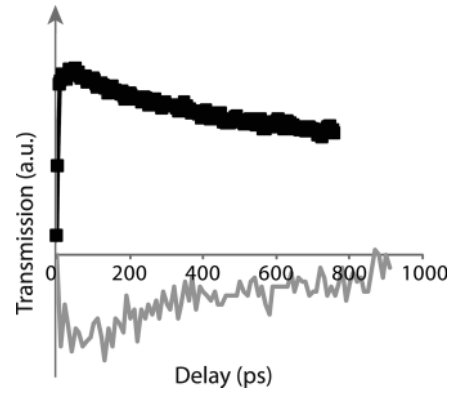

Figure 2. Transient bleaching (−■−) and intraband absorption dynamics (−) of parent CdS nanorods used in the experiments. The decay of the bleach is >4 ns and represents the ground state recovery of the system. In contrast, the decay of the intraband absorption signifies the lifetime of the electron in the $1S_e$ level and is therefore a complementary probe of the excited state dynamics.

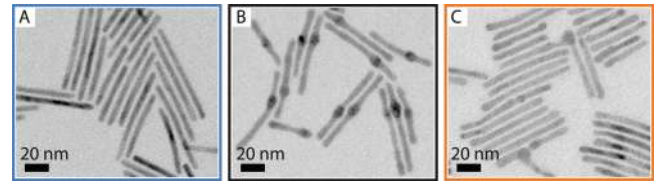

Figure 3. TEM images of CdS and Ag_2S nanorods: (A) the initial CdS nanorods; (B) Ag_2S nanorods made by full conversion of the CdS nanorods; (C) recovered CdS′ nanorods after back conversion from Ag_2S. The dark regions of the nanorods in part B are formed by partial reduction of Ag_2S under irradiation of the electron beam.[25]

between electron and hole wave functions. Good overlap as a consequence of spatial confinement can lead to a transfer of excess energy from the electron to the hole and fast intraband relaxation.[19] Second, carriers may be trapped (Figure 1C) by intrinsic surface states such as dangling bonds due to incomplete passivation of the nanocrystal surface, which is also a relatively fast process (0.1−1 ps).[20] As the Lewis basic surfactants (alkylphosphonates) used to grow and passivate the CdS nanocrystals bind much stronger to electron deficient Cd^{2+} over S^{2-}, the surface is believed to be Cd^{2+} rich.[17] Cd^{2+} ions that are not fully passivated by the alkylphosphonate ligands can lead to shallow electron traps, while S^{2-} ions at the nanocrystal surface act as sites for hole trapping.[21] Both electron and hole trapping have been observed in II−VI semiconductor nanocrystals, although their contribution to the relaxation dynamics can vary with the chemical composition of the nanocrystal, the ligands used to passivate their surface, as well as the solvent in which the nanocrystals are dispersed.[14,20,22] The degree of passivation will determine whether carriers preferentially recombine radiatively at the band edge or radiatively/nonradiatively through the trap states.

One method to characterize the relaxation of hot carriers is by monitoring the occupation of an energy level as a function of time. After photogeneration of an electron and intraband relaxation, the first excitonic transition $1S_e$ level becomes partially saturated and the transition bleaches for probe photons arriving at later times (Figure 1B). Transient bleaching experiments determine both the time it takes for the bleach to reach its maximum (i.e., the rise time, τ_{rise}, of carriers cooling to that level) and the ground state recovery time, τ_{rec}, which comprises all processes that return the system to its original state before excitation. Alternatively, a probe photon with an energy corresponding to the difference between the $1S_e$ and $1P_e$ levels can be used to monitor the intraband transition of an electron in the conduction band to obtain dynamical information about the excited state time evolution.[23]

Transient bleaching and absorption dynamics of the parent CdS nanorods used in the experiments are shown in Figure 2. The rise time of the bleach is $\tau_{rise} = 1.7 \pm 0.1$ ps and the recovery of the bleach is best fit with a biexponential decay function yielding time constants of $\tau_1 = 202 \pm 52$ ps and $\tau_2 = 3300 \pm 770$ ps. Physically speaking, the faster decay time component ($\tau_1 = 1-100$ ps) corresponds to a convolution of trapping processes while the slower ($\tau_2 = 100-1000$ ps) time component represents long-lived states. The latter pathway could be any one of the situations involving separated charges on the nanocrystal, radiative trap recombination, trap-to-trap hopping, or relaxation through a series of nonradiative levels.[24] There is evidence that low-energy trap states (from a distribution of trap states) play an especially dominant role in the longer lifetimes.[22] Also plotted in Figure 2 is the intraband absorption from the $1S_e-1P_e$ transition, where a monoexponential fitted decay constant of $\tau_{decay} = 286 \pm 81$ ps describes the electron's lifetime in the $1S_e$ level. The noticeably higher noise in the intraband signal is due to greater pulse-to-pulse fluctuations in the nonlinear optically generated mid-infrared probe. The value of τ_{decay} is comparable to that of τ_1 in the transient bleaching trace, demonstrating the correlation between the two techniques.

B. Sequential Conversion between CdS and Ag_2S Nanorods. TEM images of CdS and Ag_2S nanorods are shown in Figure 3. A molar excess of Ag^+ added to the nanorods ($Ag^+/Cd^{2+} > 2$ as two Ag^+ ions are need to replace one Cd^{2+} ion) completely converts the composition to Ag_2S, while closely preserving the dimensions of the original nanorods (Figure 3B and Figure S1 in the Supporting Information). There is an increase in the average nanorod diameter from 5.3 ± 0.4 (average ± first standard deviation) to 5.7 ± 0.5 nm and a decrease in the average nanorod length from 66 ± 14 to 58 ± 14 nm following exchange. The small change in dimensions is in part due to the difference in lattice volumes of the two crystals. Disruption of the anion framework during cation exchange can also cause partial restructuring of the nanocrystal toward a less anisotropic shape (i.e., lower surface area).[9] Some nanorods are also observed to coalesce during the transformation. To convert the Ag_2S nanocrystals back to CdS, a large excess of Cd^{2+} ions, higher temperature, and coordinating molecules with greater binding strengths to Ag^+ (i.e., MeCN and TBP) are used.[9,12,26] The reverse exchange reaction also

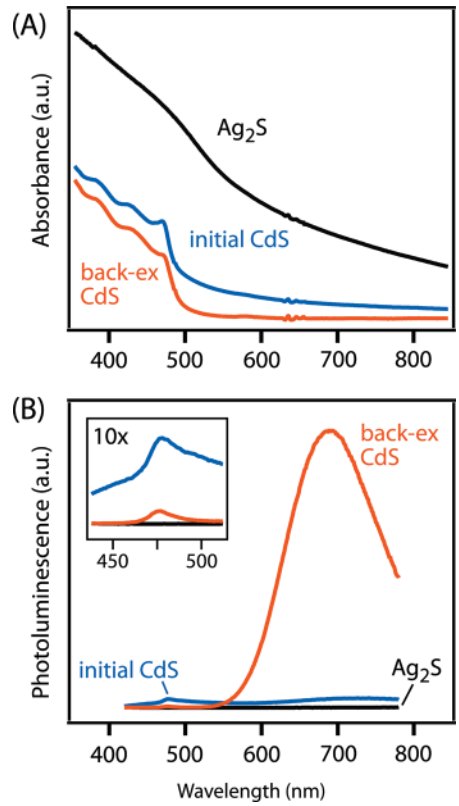

Figure 4. Absorbance and fluorescence spectra of CdS and Ag_2S nanorods: (A) absorbance spectra of CdS nanorods, converted Ag_2S nanorods, and back-exchanged CdS′ nanorods; (B) fluorescence spectra of the same samples showing the large increase in surface trap emission after sequential exchange. The inset shows the band edge emission from the CdS samples on a 10× scale. The colors of the plots match the borders of the TEM images in Figure 3 for the same samples.

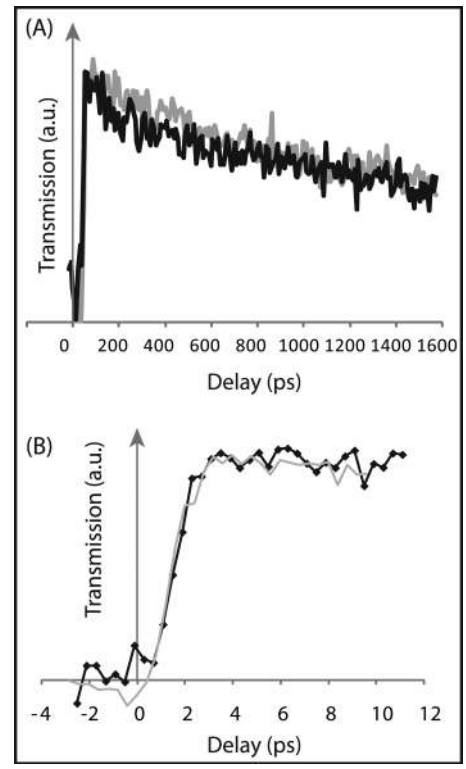

Figure 5. (A) Comparison of the transient bleach dynamics of CdS nanorods (—, gray) to the nanorods that underwent full conversion to Ag_2S followed by back exchange to CdS (—◆—, black). (B) Magnification of the dynamics at early time delays indicates that electron relaxation follows a similar pathway after forward and back exchange. The Ag_2S nanorods show no signal in these measurements.

generally preserves the nanorod morphology, where the dimensions of the recovered CdS nanorods are 5.0 ± 0.5 nm in diameter and 60 ± 14 nm in length. However, after the sequential exchange reactions, there is a larger variation in the diameter along individual nanorods.

Absorption and fluorescence spectra following the sequential exchange reactions (CdS → Ag_2S → CdS′) are shown in Figure 4. The absorption spectrum of the initial CdS nanorods displays well-defined excitonic features with the first exciton peak at ~471 nm (2.6 eV), whereas the bulk band gap, E_g, of CdS is 2.5 eV (λ = 497 nm).[27] Absorption from the fully converted Ag_2S nanocrystals is broad, with no clear excitonic features, as Ag_2S nanocrystals generally do not exhibit quantum confinement effects and possess a band gap similar to that of bulk Ag_2S (E_g ~ 1.0 eV, λ ~ 1240 nm).[28,29] However, the back conversion of the Ag_2S nanorods to CdS is accompanied by recovery of the original exciton features, with the spectral position of the first exciton peak located within 2 nm of the original CdS nanorods.

CdS nanorods exhibit both excitonic emission as well broad emission to the red of the exciton peak arising from defect states. Exciton emission occurs at 488 nm, while the broad peak centered at ~700 nm has previously been attributed to excess Cd^{2+} (i.e., S^{2-} vacancies) at the surface of the nanocrystal.[21] The Ag_2S nanorods show no emission in the visible region, although weak near-infrared emission corresponding to E_g for Ag_2S has been previously reported.[8] The fluorescence spectrum of the back-converted CdS nanorods displays greatly increased trap emission with only very weak band edge emission (Figure 4B). The quantum yields (QYs) of the exciton and trap emission in the initial CdS sample are approximately 0.1 and 5%, respectively, while the trap emission QY in the recovered CdS nanorods is approximately 30%. As the reverse exchange is performed with a large excess of Cd^{2+}, surface adsorption of these cations during exchange is expected to increase the number of electron trap states.[21] While residual Ag^+ ions within the CdS lattice or at its surface may also act as trap states, the amount of Ag^+ is expected to be low on the basis of the absorption spectra of the recovered nanorods and the bleaching dynamics described below.

Figure 5 shows transient bleaching dynamics of the initial CdS nanorods and the recovered ones after conversion to Ag_2S. The transients of the initial and recovered CdS nanorods are nearly identical at short times (delay of 0−12 ps). Biexponential fits to the decay dynamics are τ_1 = 350 ± 100 ps and τ_2 = 3200 ± 200 ps for the initial CdS nanorods and τ_1 = 100 ± 32 ps and τ_2 = 3470 ± 277 ps for the back-converted ones. The time constant, τ_1, is shorter in the recovered sample compared to the original CdS nanorods, indicating that new trap states have been introduced. The near complete recovery of the original exciton features upon back exchange dynamics suggests there is little reorganization of the anion sublattice, except near the surface of the nanocrystal, in agreement with the increase in surface trap emission after double exchange. This is quite remarkable considering the different lattice volumes of CdS and Ag_2S (~15%) as well as their different symmetries (hexagonal versus monoclinic). Thus, cation exchange is able to completely and reversibly alter the exciton dynamics of semiconductor nanocrystals, where the main effect is from the change in chemical composition, although some surface states were introduced through the process.

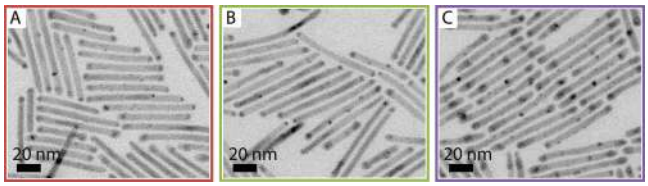

Figure 6. TEM images of CdS−Ag_2S heterostructures made with increasing Ag^+/Cd^{2+} ratios and with approximate Ag_2S/CdS volume fractions of (A) 0.12, (B) 0.19, and (C) 0.30.

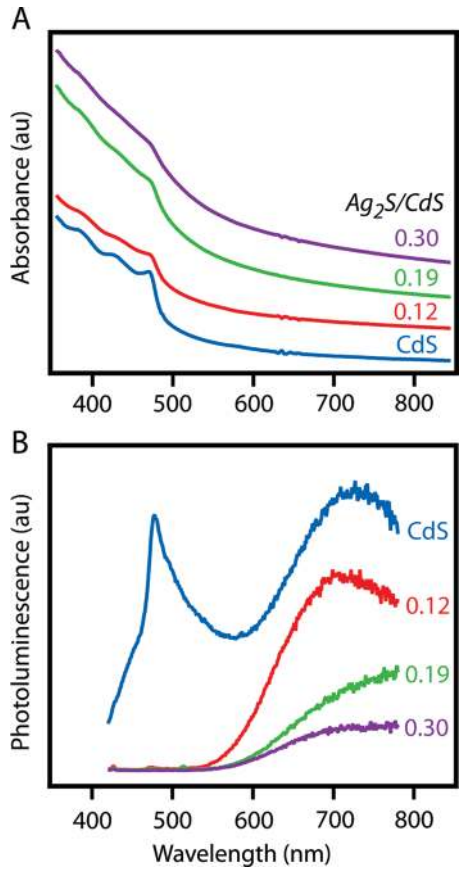

Figure 7. Absorbance and fluorescence spectra of CdS−Ag_2S nanorod heterostructures. (A) Absorbance spectra for increasing volume fractions of Ag_2S. The Ag_2S/CdS ratio is given above each plot. (B) Fluorescence spectra of the same samples showing quenching of both the CdS exciton and trap emission as the Ag_2S fraction increases. The colors of the plots match the borders of the TEM images in Figure 6 for the same samples.

C. Exciton Dynamics of CdS−Ag_2S Nanorod Heterostructures. After evaluating how the cation exchange reaction affects carrier dynamics through the introduction of surface states (see previous section), we can now look at the dynamics of CdS−Ag_2S heterostructures made with varying Ag^+/Cd^{2+} ratios to control the relative volume fraction of Ag_2S within the nanorods. TEM images of the heterostructures are shown in Figure 6, where the regions of Ag_2S formed within the CdS nanorods appear as darker spots, as the Ag_2S lattice has a greater atomic density. The volume fraction of Ag_2S within the nanorods grows larger as the Ag^+/Cd^{2+} ratio used in the exchange reactions is increased.[8] The approximate volume fractions of Ag_2S within the nanorods are 0.12, 0.19, and 0.30 as measured from the TEM images. Absorbance and fluorescence spectra for the CdS−Ag_2S nanorods are shown in Figure 7. For increasing amounts of Ag^+ added, an absorption tail to the red of the CdS band edge grows stronger in intensity due to the presence of the smaller band gap Ag_2S material (Figure 7A).

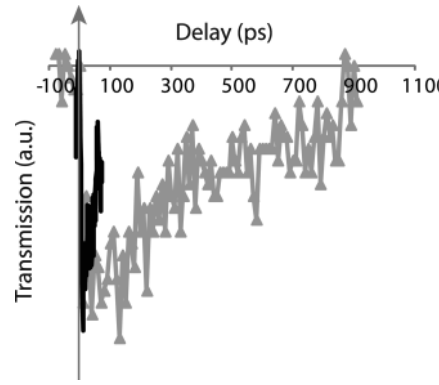

Figure 8. Intraband absorption dynamics of CdS nanorods (−▲−) compared to a representative trace (−) of cation-exchanged nanorods. All of the cation-exchanged samples exhibit significantly faster decay than that of the initial CdS nanorods, which suggests that electron relaxation pathways are created in the Ag_2S regions.

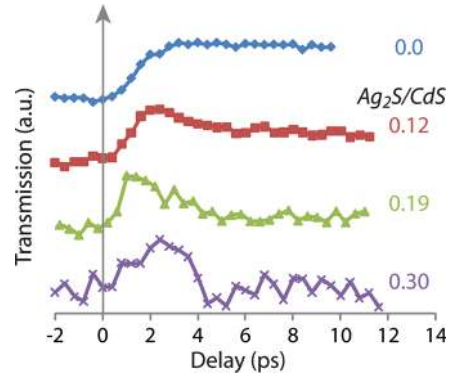

Figure 9. Normalized and offset transient bleaching traces of the $1S_e$ transition as a function of Ag_2S fraction: Ag_2S /CdS = 0.0 (−◆−), Ag_2S/CdS = 0.12 (−■−), Ag_2S/CdS = 0.19 (−▲−), and Ag_2S /CdS = 0.30 (−×−). As the fraction of Ag_2S increases in the nanorods, the contribution from the fast time component τ_1 of the transient bleach recovery also increases until it dominates the dynamics at 0.30 exchange. Higher exchange fractions show little signal due to the small amount of CdS they contain.

However, the spectral position of the first CdS exciton feature at 470 nm remains the same, indicating that there is little change in the average nanorod diameter during the reaction.[30] The fluorescence spectra show that, even for low fractions of exchange, exciton emission from the CdS material is quenched. Surface trap emission from CdS is still present in the heterostructures but becomes weaker in intensity as the Ag_2S regions grow in size. Because the Ag_2S material forms near the surface of the CdS nanorod for low fractions of exchange, its presence may partially remove radiative surface traps. The absence of band edge emission and decrease in trap emission suggest that new relaxation processes are made available by the presence of Ag_2S within the nanorods which occur on a much faster time scale than radiative recombination.

Intraband absorption ($1S_e$−$1P_e$) dynamics of CdS nanorods subject to varying degrees of cation exchange all yield a similar trace shown in Figure 8. That is, the intraband decay constants (τ_{decay} = 7−22 ps) of the CdS−Ag_2S heterostructures are significantly faster than that of the parent CdS nanorods. We can gain a clearer understanding of the pathways with transient bleaching data shown in Figure 9. Not only is the electron leaving the $1S_e$ state faster (as shown by the intraband dynamics), but it is also recovering the ground state more quickly as the fast component of the bleach decay, τ_1, decreases by 2 orders of magnitude (=1.1−1.4 ps) in the heterostrucutures

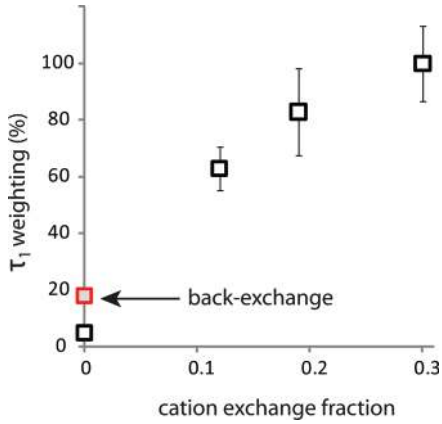

Figure 10. Fitting the transient bleach recovery to a biexponential yields a weighting of the τ_1 time component, which represents an electron trapping pathway in the nanorods and a pathway to Ag_2S regions and interfacial defect states in the cation-exchanged systems. The exchange of fully converted Ag_2S back to CdS nearly recovers the original weighting of τ_1. Note that τ_1 is on the order of 100 ps in both CdS samples and 1 ps in the heterostructures.

compared to the initial CdS nanorods. Biexponential fits to the bleaching decay curves show that the weighting of τ_1 increases as the volume fraction of Ag_2S increases (Figure 10). The long-lived states present in the original CdS nanorods are no longer the dominant relaxation pathways; instead, fast trapping of both electrons and holes followed primarily by nonradiative recovery of the ground state occurs. In addition, the rise times of the 0.19-exchange ($\tau_{rise} = 0.76 \pm 0.14$ ps) and 0.30-exchange ($\tau_{rise} = 0.76 \pm 0.14$ ps) samples are faster than that of the parent CdS nanorods ($\tau_{rise} = 1.2 \pm 0.3$ ps). Greater overlap of the electron and hole wave functions in CdS occurs once the Ag_2S regions span the diameter of the nanorod, thus separating segments of CdS within the nanorods.

The faster decay dynamics in the heterostructures potentially arise from three different sources: (1) New defect states at the CdS surface may be formed as a result of the cation exchange process. However, in the full exchange experiments, increasing disorder at the surface leads to an increase in radiative trap emission (Figure 4B) rather than a decrease as observed for partial exchange. (2) Interfacial defects between CdS and Ag_2S can exist due to the relatively large lattice mismatch between these two crystals, which can act as trap sites.[8,16] As the Ag_2S material grows into the CdS lattice, the elastic strain between the two lattices will increase, possibly leading to more interfacial defects. (3) The conduction and valence band edges of Ag_2S are both predicted to be within the band gap of CdS (type I level alignment).[8] Therefore, excited electrons can either relax from the conduction band edge of CdS into the Ag_2S conduction band followed by relaxation back to the CdS valence band or alternatively participate in energy transfer—via Coulombic or Förster-type transfers—to Ag_2S, considering that the band alignment should create good spectral overlap and electronic coupling between the two materials. While Förster energy transfer between quantum dots are normally observed at a longer time scale (tens of picoseconds to nanoseconds), the epitaxial connection between the CdS and Ag_2S lattices could lead to shorter transfer times.[31]

The original energy scheme and carrier relaxation pathway from Figure 1 is modified for the Ag_2S−CdS heterostructures. Figure 11 shows the proposed pathways based on the static and transient optical experiments characterized in this work. Partial cation exchange to make CdS−Ag_2S heterostructures creates

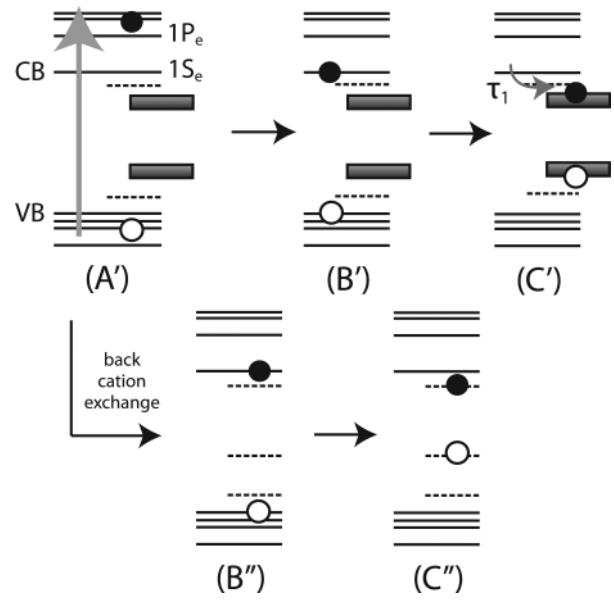

Figure 11. Proposed energy level schemes and relaxation pathways of cation-exchanged Ag_2S−CdS nanorods. The darkened regions in part A′ depict new electron and hole trapping pathways created by regions of Ag_2S. Electrons (B′) relax to the band edge in τ_{rise} as before but (C′) trap to Ag_2S states in τ_1. Back exchange from Ag_2S to CdS (B″) anneals the majority of deep traps, but (C″) some remain, as evidenced by photoluminescence spectra in Figure 4B and weighting of τ_1 from Figure 10.

new levels within the band gap of CdS, which include both interfacial defects as well as the Ag_2S conduction and valence bands. This leads to very fast relaxation of excited electrons in the CdS conduction band as probed by both their disappearance from the excited state and their recovery to the ground state. Sequential cation exchange reactions change the dynamics primarily by introducing new trap states at the surface of the nanocrystals.

One shortcoming of the transient experiments is that it is not possible to further characterize the nature of the long-lived trap states, which show up only as a nanosecond decay in the transient bleach recovery; their negligible transition dipole moments preclude a direct optical probe of the trap state dynamics. Another limitation to the analysis of this particular system is that, once the electron is shuttled away from the $1S_e$ state, it is unclear whether it eventually resides in a deep trap or nonradiatively decays within regions of Ag_2S. If the fluorescence quantum yield of these structures could be improved, then time-resolved photoluminescence experiments—shown previously to be sensitive to the presence and type of trap states—may provide a way to further characterize the relaxation process.[14,22] Recently, both carrier trapping and charge transfer to the surface ligands in semiconductor nanocrystals have been modeled using Marcus electron transfer theory.[22,32] Such a model may also be applicable to the CdS−Ag_2S system and could be used to differentiate between the proposed relaxation pathways of excited carriers described above.

IV. Conclusion

Exciton dynamics were studied in CdS−Ag_2S nanorods to characterize how the process of cation diffusion and the presence of a secondary material within the nanocrystal lattice affect the relaxation of excited photoexcited carriers. The type I electronic band alignment between CdS and Ag_2S combined with the morphology of small Ag_2S regions embedded within the CdS

nanorods provides an interesting structure where visible light absorption in the wide band gap CdS material can produce near-infrared emission from the narrow gap Ag_2S. While the fast decay dynamics in the heterostructures suggest strong electronic coupling between the CdS and Ag_2S materials, it also indicates there is a significant amount of trap states (most likely interfacial defects), which prevent radiative recombination from the Ag_2S band edges. One way to solve this problem may be to change the composition of the heterostructure, while preserving its morphology. For instance, we have recently shown that the CdS−Ag_2S nanorod heterostructures can be converted to CdS−PbS nanorods by a second exchange reaction.[26] PbS also has a highly tunable direct band gap in the near-infrared which may improve the quantum yield of these types of nanocrystal heterostructures.[7] Cation exchange provides a powerful route for tuning the composition and resulting optical properties of ionic semiconductor nanocrystals. Further studies on the carrier dynamics in these materials can facilitate their application in optoelectronic devices for light absorption (e.g., photovoltaics) and emission (e.g., light-emitting diodes and lasers).

Acknowledgment. The authors thank Dr. Gordana Dukovic and Dr. Prashant K. Jain for helpful discussions in preparing the manuscript and Maxwell Merkle for measurement of nanorod concentrations. The nanocrystal synthesis portion of this work, carried out by B.S. and supervised by A.P.A. and R.J.S., was supported by the Director, Office of Science, Office of Basic Energy Sciences, Chemical and Materials Sciences Divisions, of the U.S. Department of Energy under Contract No. DE-AC02-05CH1123. The spectroscopy experiments, carried out by P.P. and supervised by R.J.S., were supported by the Experimental Physical Chemistry Division of the National Science Foundation under Grant No. CHE-0650950. P.P. was supported by the NSF-IGERT foundation.

Supporting Information Available: Detailed descriptions of the CdS nanorod synthesis and cation exchange reactions, size histograms of the nanorods, and transient bleaching and intraband absorption dynamics of the nanorods in the presence of chemical quenchers. This material is available free of charge via the Internet at http://pubs.acs.org.

References and Notes

(1) Bailey, R. E.; Nie, S. M. *J. Am. Chem. Soc.* **2003**, *125*, 7100–7106.
(2) Pradhan, N.; Goorskey, D.; Thessing, J.; Peng, X.-G. *J. Am. Chem. Soc.* **2005**, *127*, 17586–17587.
(3) Zhong, X.-H.; Feng, Y.-Y.; Zhang, Y.-L.; Gu, Z.-Y.; Zhou, L. *Nanotechnology* **2007**, *18*, 385606.
(4) Kim, S.; Fisher, B.; Eisler, H.-J.; Bawendi, M. *J. Am. Chem. Soc.* **2003**, *125*, 11466–11467.
(5) Battaglia, D.; Blackman, B.; Peng, X.-G. *J. Am. Chem. Soc.* **2005**, *127*, 10889–10897.
(6) Mews, A.; Eychmuller, A.; Giersig, M.; Schoss, D.; Weller, H. *J. Phys. Chem.* **1994**, *98*, 934–941.
(7) Pietryga, J. M.; Werder, D. J.; Williams, D. J.; Casson, J. L.; Schaller, R. D.; Klimov, V. I.; Hollingsworth, J. A. *J. Am. Chem. Soc.* **2008**, *130*, 4879–4885.
(8) Robinson, R. D.; Sadtler, B.; Demchenko, D. O.; Erdonmez, C. K.; Wang, L.-W.; Alivisatos, A. P. *Science* **2007**, *317*, 355–358.
(9) Son, D.-H.; Hughes, S. M.; Yin, Y.-D.; Alivisatos, A. P. *Science* **2004**, *306*, 1009–1012.
(10) Sadtler, B.; Demchenko, D. O.; Zheng, H.; Hughes, S. M.; Merkle, M. G.; Dahmen, U.; Wang, L.-W.; Alivisatos, A. P. *J. Am. Chem. Soc.* **2009**, *131*, 5285–5293.
(11) Wark, S. E.; Hsia, C.-H.; Son, D.-H. *J. Am. Chem. Soc.* **2008**, *130*, 9550–9555.
(12) Camargo, P. H. C.; Lee, Y.-H.; Jeong, U.; Zou, Z.-Q.; Xia, Y. *Langmuir* **2007**, *23*, 2985–2992.
(13) Chan, E. M.; Marcus, M. A.; Fakra, S.; ElNaggar, M.; Mathies, R. A.; Alivisatos, A. P. *J. Phys. Chem. A* **2007**, *111*, 12210–12215.
(14) Garrett, M. D.; Dukes, A. D., III; McBride, J. R.; Smith, N. J.; Pennycook, S. J.; Rosenthal, S. J. *J. Phys. Chem. C* **2008**, *112*, 12736–12746.
(15) Samia, A. C. S.; Lou, Y.; Burda, C.; Senter, R. A.; Coffer, J. L. *J. Chem. Phys.* **2004**, *120*, 8716–8723.
(16) Demchenko, D. O.; Robinson, R. D.; Sadtler, B.; Erdonmez, C. K.; Alivisatos, A. P.; Wang, L.-W. *ACS Nano* **2008**, *2*, 627–636.
(17) Owen, J. S.; Park, J.; Trudeau, P.-E.; Alivisatos, A. P. *J. Am. Chem. Soc.* **2008**, *130*, 12279–12281.
(18) Jones, G.; Jackson, W. R.; Halpern, A. M. *Chem. Phys. Lett.* **1980**, *72*, 391–395.
(19) Klimov, V. I. *J. Phys. Chem. B* **2000**, *104*, 6112–6123.
(20) Burda, C.; Link, S.; Mohamed, M.; El-Sayed, M. *J. Phys. Chem. B* **2001**, *105*, 12286–12292.
(21) Ramsden, J. J.; Gratzel, M. *J. Chem. Soc., Faraday Trans. 1* **1984**, *80*, 919–933.
(22) Jones, M.; Lo, S.-S.; Scholes, G. D. *Proc. Natl. Acad. Sci. U.S.A.* **2009**, *106*, 3011–3016.
(23) Guyot-Sionnest, P.; Shim, M.; Matranga, C.; Hines, M. *Phys. Rev. B* **1999**, *60*, R2181–R2184.
(24) Cavaleri, J. J.; Skinner, D. E.; Colombo, D. P.; Bowman, R. M. *J. Chem. Phys.* **1995**, *103*, 5378–5386.
(25) Motte, L.; Urban, J. *J. Phys. Chem. B* **2005**, *109*, 21499–21501.
(26) Luther, J. M.; Zheng, H.; Sadtler, B.; Alivisatos, A. P. *J. Am. Chem. Soc.* **2009**, *131*, 16851–16857.
(27) Ninomiya, S.; Adachi, S. *J. Appl. Phys.* **1995**, *78*, 1183–1190.
(28) Huxter, V. M.; Mirkovic, T.; Nair, P. S.; Scholes, G. D. *Adv. Mater.* **2008**, *20*, 2439–2443.
(29) Junod, P.; Hediger, H.; Kilchor, B.; Wullschleger, J. *Philos. Mag.* **1977**, *36*, 941–958.
(30) Li, L.-S.; Hu, J.-T.; Yang, W.-D.; Alivisatos, A. P. *Nano Lett.* **2001**, *1*, 349–351.
(31) Achermann, M.; Petruska, M. A.; Crooker, S. A.; Klimov, V. I. *J. Phys. Chem. B* **2003**, *107*, 13782–13787.
(32) Hyun, B.-R.; Bartnik, A. C.; Lee, J.-K.; Imoto, H.; Sun, L.-F.; Choi, J.-J.; Hanrath, T.; Ober, C. K.; Wise, F. W. *Nano Lett.* **2010**, *10*, 318–323.

JP9116722